THE JOURNAL OF PHYSICAL CHEMISTRY C

Article

Cite This: J. Phys. Chem. C 2019, 123, 29116−29125

pubs.acs.org/JPCC

Sterically Controlled Excited-State Intramolecular Proton Transfer Dynamics in Solution

Jungkweon Choi,[†,‡,⊥] Doo-Sik Ahn,[†,‡,⊥] Sol-Yi Gal,[§] Dae Won Cho,[∥] Cheolhee Yang,[†,‡] Kyung-Ryang Wee,[*,§] and Hyotcherl Ihee[*,†,‡]

[†]Center for Nanomaterials and Chemical Reactions, Institute for Basic Science, Daejeon 34141, Republic of Korea

[‡]Department of Chemistry and KI for BioCentury, Korea Advanced Institute of Science and Technology (KAIST), Daejeon 305-701, Republic of Korea

[§]Department of Chemistry and Institute of Natural Science, Daegu University, Gyeongsan 38453, Republic of Korea

[∥]Department of Advanced Materials Chemistry, Korea University, Sejong Campus, Sejong 30019, Korea

Supporting Information

ABSTRACT: Excited-state intramolecular proton transfer (ESIPT) is a fundamental ultrafast photochemical process. Although it has been intensively studied for the development of novel photonic devices such as organic light-emitting diodes, the relation between ESIPT reaction and intramolecular charge transfer (ICT) is still a subject of debate. Furthermore, the effects of the molecular geometry and of the substituent on ESIPT and ICT processes are still unclear. To address these issues, we synthesized a set of four compounds designed to control the electron density distribution of the proton-donating (PD) group and the steric hindrance between the PD and the adjacent phenyl groups: three 2-(1-phenyl-1*H*-imidazo[4,5-*f*][1,10]phenanthrolin-2-yl)phenol derivatives, PIPP-Xs (X = H, F, and OMe), and 2-(1-phenyl-1*H*-imidazo[4,5-*f*][1,10]phenanthrolin-2-yl)naphthalen-2-ol (PIPN). We then investigated their ESIPT and ICT dynamics as well as the related structural changes using femtosecond transient absorption spectroscopy and theoretical calculations. Although the four compounds commonly exhibit a dual emission originating from the excited enol (E*) and keto (K*) tautomers, their emission properties, such as emission maxima and lifetimes, are systematically modulated by substitution at the para-position of the PD group. The experimental and time-dependent density functional theory calculation results showed that the substitution of an electron-withdrawing group at the para-position of the PD group and the planarity between the PD and proton-accepting (PA) groups play important roles in inducing an efficient ESIPT characterized by increased emission of the K* tautomer. On the other hand, the photoexcitation for PIPP-Xs induces the formation of *cis*-K*, which is the most stable structure, whereas in PIPN the E* tautomer generated by the photoexcitation is rapidly converted to two species, *cis*-K* and *per*-K* with time constants of <0.2 and 0.5 ps, respectively. Furthermore, the *per*-K* state of PIPN has a charge transfer characteristic, suggesting intramolecular charge migration induced by the formation of *per*-K* state. This distinctive dynamics of PIPN is due to its pretwisted structure between PD and PA groups. The results provided in this study demonstrate that the molecular geometry plays an important role in the ESIPT and ICT processes.

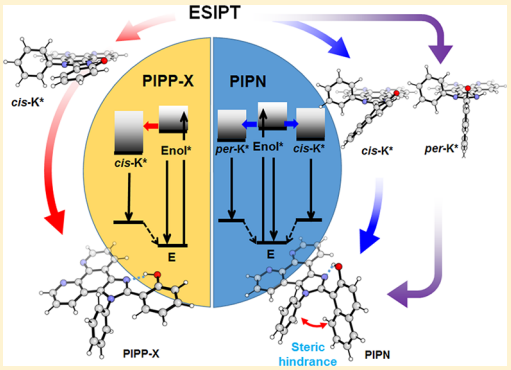

INTRODUCTION

Excited-state intramolecular proton transfer (ESIPT), which is observed in a molecule with pre-existing intramolecular hydrogen bonding, has received much attention as an important photophysical property for potential applications such as molecular probes,[1−4] optoelectronic materials,[5−8] molecular logic gates,[2,9] and sensor devices.[10,11] Because ESIPT reactions strongly depend on many factors such as solvent, substituents, and molecular structures, various compounds have been extensively studied in numerous experimental and theoretical approaches to understand the ESIPT process and subsequent reaction dynamics as well as to tune the optical responses such as fluorescence and phosphorescence as a photonic material.[1,2,12,13]

The ESIPT process, which induces phototautomerization from the excited enol form (E*) to the keto form (K*) (Figure 1a), occurs rapidly, on the subpicosecond time scale, and results in dual emission from E* and K* tautomers. The process of E* → K* phototautomerization accompanies large Stokes shift, which is an important photophysical characteristic of ESIPT dynamics. Meanwhile, it has been reported that in

Received: August 2, 2019
Revised: November 4, 2019
Published: November 6, 2019

DOI: 10.1021/acs.jpcc.9b07373
J. Phys. Chem. C 2019, 123, 29116−29125

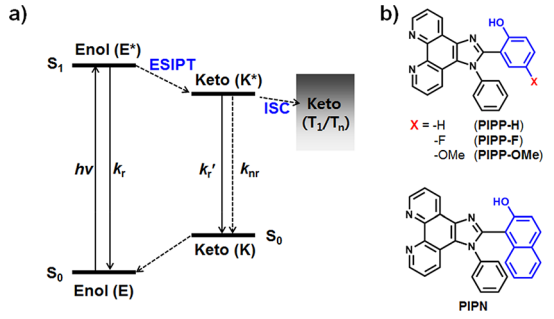

Figure 1. (a) Energy diagram for the ESIPT process. k_r and k_{nr} are the decay rates for radiative and nonradiative transition, respectively. (b) Structures of four ESIPT compounds, three PIPP-Xs, and PIPN; 2-(1-phenyl-1*H*-imidazo[4,5-*f*][1,10]phenanthrolin-2-yl)phenol (PIPP-H), 4-fluoro-2-(1-phenyl-1*H*-imidazo[4,5-*f*][1,10]phenanthrolin-2-yl)phenol (PIPP-F), 4-methoxy-2-(1-phenyl-1*H*-imidazo[4,5-*f*][1,10]phenanthrolin-2-yl)phenol (PIPP-OMe), and 1-(1-phenyl-1*H*-imidazo[4,5-*f*][1,10]phenanthrolin-2-yl)naphthalen-2-ol (PIPN). Blue-colored molecular frame represents the PD group for ESIPT.

ESIPT compounds with an electron donor or acceptor group, the proton transfer is strongly coupled with the intramolecular charge-transfer (ICT) process. Chou and Douhal groups have demonstrated the cooperative or competitive interplay of IPT (intramolecular proton transfer) and ICT on ESIPT dynamics by introducing substituents on proton donating or accepting groups as well as by changing the solvent environment such as solvent polarity and viscosity.[14−20] However, despite numerous experimental and theoretical studies, the charge-transfer dynamics induced by the ESIPT reaction is still elusive. Seo et al. reported that the strong positive solvatochromic shift measured for 2-(2′-hydroxyphenyl)benzoxazole (HBO) derivatives with conjugative electron acceptors is due to the consecutive ESIPT and ICT processes.[21] In contrast, Chou et al. showed that in 4-(dimethylamino)-1*H*-pyrrolo[2,3-*b*]-pyridine, the proton transfer follows after ICT and the dual excitation behavior (ICT vs proton transfer) is fine-tuned by solvent polarity and hydrogen-bonding ability.[22] Recently, using femtosecond Kerr-gated spectroscopy, Rumble et al. showed that the ESIPT reaction in 4′-*N*,*N*-diethylamino-hydroxyflavone is correlated with the solvation time.[23] These results show that there is no clear consensus on ICT induced by ESIPT.

Besides ICT induced by ESIPT, the effects of molecular geometry and substituent on ESIPT and ICT processes are still unclear. E* → K* phototautomerization can cause a remarkable structural change because the electron density distribution of K* is significantly different from that of E*. It has been suggested that the structural change induced by E* → K* phototautomerization is influenced by the ground-state geometry as well as by the substituents on the proton-donating (PD) or proton-accepting (PA) group. In particular, because the ground-state geometry determines the starting point on the potential energy surface for the ESIPT reaction, the so-called Frank−Condon (FC) state, the relationship between the ground state geometry and ESIPT dynamics has been investigated to allow a mechanistic understanding of the ESIPT processes, including the tunneling dynamics.[24−27] In addition, the rotational isomerism of E* and K* tautomers has been widely investigated for understanding of the emission mechanism and to improve the emission quantum yield. Recently, the effect of twisted ICT (TICT) of K* following ESIPT has been intensively investigated as a crucial factor determining the emission efficiency in solution and solid state.[13] In solution, for example, the twisted K* structure from ESIPT provides efficient pathways for fluorescence quenching of K* via radiationless relaxation to the ground state or triplet state, whereas the restricted twisting of the K* tautomer in rigid media such as crystals shows a significant emission.[13] Moreover, the effects of steric hindrance on the ESIPT dynamics and on the emission efficiencies have been studied as well. Iijima et al. reported the photophysical properties of naphthalene-fused 2-(2′-hydroxyaryl)benzazole dyes and discussed the effects of bulky naphthalene-based chromophore on the ESIPT dynamics and subsequent twisting.[28]

To elucidate the effects of molecular geometry and substituent on ESIPT and the subsequent relaxation dynamics, such as ICT, we synthesized a set of four compounds with varying substituents designed to control the electron density distribution of the PD group and the steric hindrance between the PD and adjacent phenyl groups; these compounds were three 2-(1-phenyl-1*H*-imidazo[4,5-*f*][1,10]phenanthrolin-2-yl)phenol derivatives (PIPP-H, PIPP-F, PIPP-OMe) and 2-(1-phenyl-1*H*-imidazo[4,5-*f*][1,10]phenanthrolin-2-yl)-naphthalen-2-ol (PIPN) (see Figures 1b and S1−S4). We investigated their ESIPT and ICT dynamics using various spectroscopic techniques and theoretical calculations. The 2-(2′-hydroxyphenyl)benzothiazole (HBT) families have been extensively investigated as a prototypical framework for studying ESIPT.[29−34] In PIPP-Xs (X = H, F, and OMe), which are similar to HBO and HBT derivatives, 2-(1-phenyl-1*H*-imidazo[4,5-*f*][1,10]phenanthrolin-2-yl) and substituted 2-hydroxyphenyl moieties act as PA and PD groups, respectively. Fluorine and methoxy groups are substituted at the para-position of the PD group to modulate its electron density distribution (see Figure 1b). In PIPN, the naphthalen-2-ol group is introduced as a PD group to enrich the electron density on the PD group and to provide large steric hindrance to the adjacent phenyl moiety. The results provided herein demonstrate that the ESIPT dynamics is systematically modulated by substituents in the para-position of the PD group and that the molecular geometry plays an important role in the ESIPT and ICT processes.

RESULTS AND DISCUSSION

To characterize the spectroscopic responses of the four compounds, we first measured the steady-state absorption and emission spectra. Figure 2 shows the UV−vis absorption and emission spectra measured in dichloromethane (DCM). The absorption spectra of PIPP-Xs (X = H, F, and OMe) show similar absorption bands corresponding to the S_0-S_1 transition at around 331, 340, and 352 nm, respectively, whereas PIPN with a naphthalen-2-ol as the PD group exhibits more largely red-shifted and vibronically structured absorption bands than those of the other three compounds (Figure 2a). On the other hand, upon excitation at 350 nm, all four compounds show dual emission bands, which have maxima in the 400 and 500 nm regions (Figure 2b). The emission quantum yields (Φ_f) of PIPP-H, PIPP-F, PIPP-OMe, and PIPN are determined to be 0.067, 0.149, 0.004, and 0.253, respectively. Because dual emission is a typical spectroscopic characteristic of ESIPT compounds, we can estimate that the ESIPT process efficiently occurs in these four compounds. Based on the four-level energy scheme for the ESIPT process (Figure 1a), the shorter- and longer-wavelength emissions of the four compounds

DOI: 10.1021/acs.jpcc.9b07373
J. Phys. Chem. C 2019, 123, 29116−29125

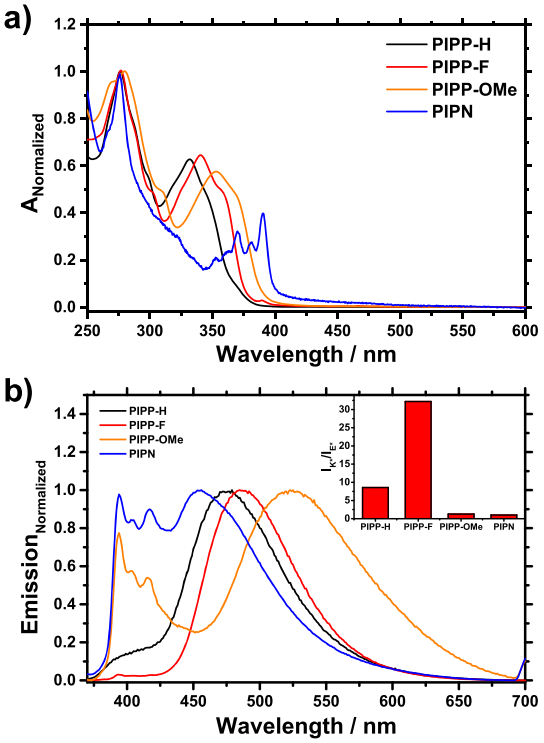

Figure 2. UV−vis absorption (a) and emission (b) spectra of four ESIPT compounds (PIPP-H, PIPP-F, PIPP-OMe, and PIPN) measured in DCM. Excitation wavelength is 350 nm. The inset in (b) shows the intensity ratios of the E* and K* bands, I_{K^*}/I_{E^*}, for the four ESIPT compounds (PIPP-H, PIPP-F, PIPP-OMe, and PIPN).

(PIPP-H, PIPP-F, PIPP-OMe, and PIPN) are attributed to those from the excited enol (E*) tautomer and excited keto (K*) tautomer, respectively. In PIPP-Xs, furthermore, the relative intensities of the emissions from the E* and K* tautomers show significant dependence on the substituents of the PD group. The substitution of an electron-withdrawing group such as fluorine (F) at the para-position of the PD group induces a strong emission from the K* tautomer, whereas the substitution of an electron-donating group such as methoxy results in a decrease of emission from the K* tautomer. The ratios of emission intensity of the E* and K* tautomers, I_{K^*}/I_{E^*}, exhibit the following order: PIPP-F ≫ PIPP-H ≫ PIPP-OMe ≥ PIPN (Figure 2b). This order indicates that the electron-withdrawing group promotes an efficient ESIPT to form K* tautomer, whereas the electron-donating group relatively suppresses the ESIPT reaction, leading to weak emission from the K* tautomer. This result indicates that the relative emission intensity from the K* tautomer correlates with acidity change of the PD group by the substituent. For example, as observed in PIPP-F, the increased acidity of the PD group by introduction of the electron-withdrawing substituent induces an efficient ESIPT reaction.

Generally, expansion of an aromatic ring in a molecule induces a red shift in the UV−vis absorption and emission spectra. In this regard, it is noteworthy that the emission from the K* tautomer of PIPN with a longer conjugated system is observed at a shorter wavelength than those of PIPP-Xs, whereas the absorption band of PIPN is red-shifted to a longer wavelength than those of PIPP-Xs. A similar phenomenon was observed by Iijima et al., who reported that compared with the emission spectrum of 2-(2′-hydroxyphenyl)benzazole compound, the introduction of naphthalen-2-ol as the PD group induces blue-shifted emission owing to the large energy gap between the ground and excited states of K*.[28] However, no explanation was given for the large energy gap between the ground and excited states for K*.

In an attempt to provide an explanation for the large energy gap between the ground and excited states for K* of PIPP-Xs (X = H, F, and OMe) and PIPN, we used the density functional theory (DFT) and time-dependent density functional theory (TDDFT) methods to calculate the minimum energy structures of enol and keto tautomers in the ground (S_0) and first excited states (S_1), respectively. The optimized structures and their relative energy levels are shown in Figures 3 and S5, and Table S1. As shown in Figure 3a, because the steric hindrance between PD and phenyl groups may induce the conformational isomerism, the twisting angle of PA and PD groups and the dihedral angle of the phenyl group with respect to the plane of imidazole ring, θ(CCCN) and θ(CCNC), are geometrical indicators to describe the conformational isomers in PIPP-Xs and PIPN. As shown in Figure 3b, in the ground state, each optimized structure of PIPP-Xs exhibits planar geometry, θ(CCCN) = 0°, whereas the optimized structure of PIPN is largely twisted, with θ(CCCN) = 51.3°. Our calculation results reveal that the large rotation of the PD group in PIPN is induced by the strong steric hindrance between naphthalen-2-ol and the adjacent phenyl groups in PIPN, resulting in relatively weak intramolecular hydrogen bonding compared with the cases of PIPP-Xs. Indeed, the intramolecular hydrogen bond length (R_{N-H}) between N and H, R_{N-H} = 2.025 Å, in PIPN is much longer than that in PIPP-H, R_{N-H} = 1.636 Å, but the H atom of the hydroxyl in the PD group is still directed to the N atom of the imidazole ring. It is worthwhile to note that in the four ESIPT compounds, no stable keto tautomer was found in the ground state. On the one hand, in the S_1 state, each PIPP-X has four optimized structures, which are attributed to one E* tautomer and three rotational isomers of the K* tautomer. The three rotational isomers of the K* tautomer can be distinguished by the degree of the twisting angle of the PD and PA groups (θ(CCCN)), which are denoted as *cis*-K* (θ(CCCN) < 80°), *per*-K* (80° < θ(CCCN) < 120°), and *trans*-K* (θ(CCCN) > 120°). Similar to the ground-state structure, the E* tautomers of PIPP-Xs in the S_1 state have a planar geometry, whereas the PD group in the optimized geometry of *cis*-K* is slightly twisted. The θ(CCCN) values for *cis*-K* of PIPP-H, PIPP-F, and PIPP-OMe are 17.1°, 17.1°, and 13.7°, respectively. In contrast to PIPP-Xs, the TDDFT calculations for PIPN in the S_1 state shows three optimized structures, namely, one twisted E* tautomer and two rotational isomers of K* tautomer corresponding to *cis*-K* and *per*-K*, as shown in Figure 3c. No optimized structure attributed to *trans*-K* was found in PIPN. The θ(CCCN) values for E*, *cis*-K*, and *per*-K* of PIPN are 25.4°, 39.7°, and 106.6°, respectively. We note that the θ(CCCN) values for E* and *cis*-K* are smaller than that for the enol form in the ground state. This is due to the shortened CC_{twist} bond in E* and *cis*-K*, which has a partial double-bond character, upon the HOMO−LUMO transition for the S_1 state to form E* and *cis*-K* (see Figures 3, S5, and S10). In addition, the θ(CCNC)s of the E* and *cis*-K* tautomers are significantly reduced compared with those of the corresponding tautomers in PIPP-H. These calculation results suggest that steric hindrance between the large PD group,

DOI: 10.1021/acs.jpcc.9b07373
J. Phys. Chem. C 2019, 123, 29116−29125

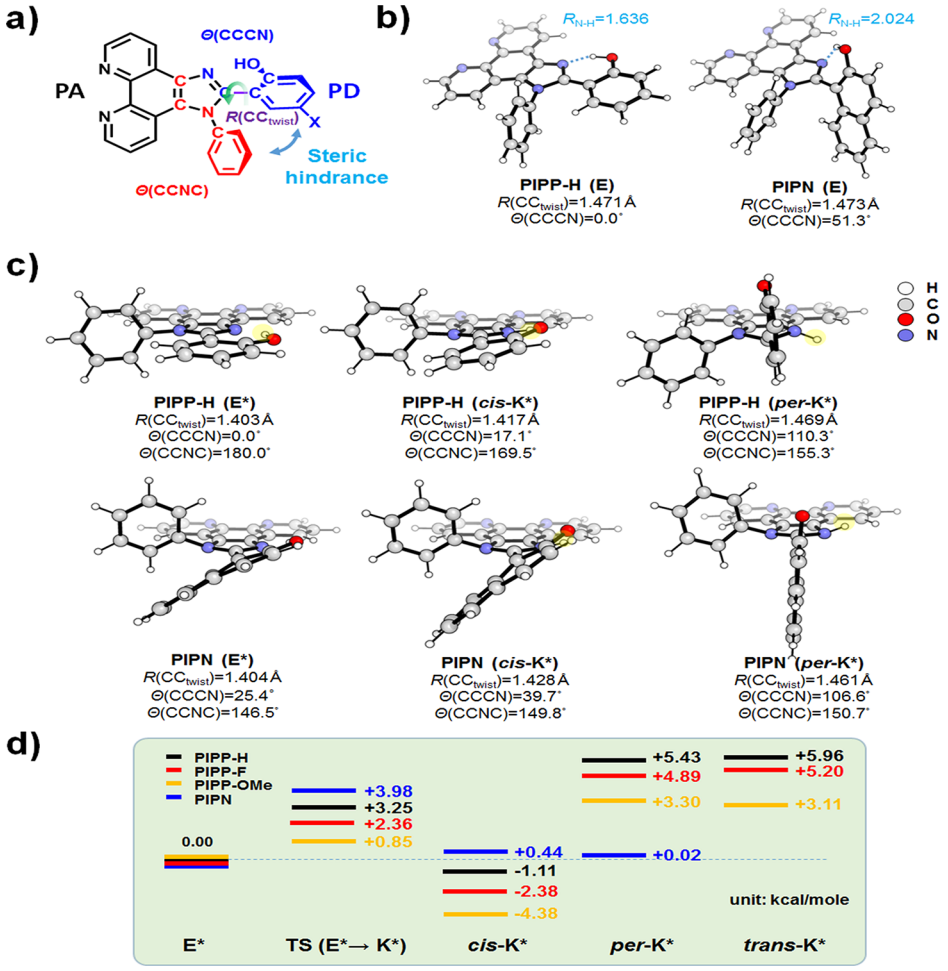

Figure 3. DFT and TDDFT calculated ground and excited structures and relative energy level diagram for E* and K* tautomers: (a) molecular framework for PIPP-Xs and important geometry parameters; R(CCtwist): the carbon−carbon bond connecting PA and PD moieties, θ(CCCN): a twisting angle between PA and PD moieties, and θ(CCNC): a dihedral angle of phenyl with respect to the imidazole ring in PA moieties; (b) calculated ground state structures of PIPP-H and PIPN; (c) TDDFT optimized S1 state structures of enol and keto-forms of PIPP-H (upper) and PIPN (bottom), including *cis*-K* (θ(CCCN) < 80°), *per*-K* (80° < θ(CCCN) < 120°), and *trans*-K* (θ(CCCN) > 120°). The yellow-shaded circle indicates the position of hydrogen atom for ESIPT; (d) relative energy levels of K* tautomers and transition state for ESIPT compared to E* energy in all ESIPT compounds.

naphthalen-2-ol, and the phenyl group in PIPN is much stronger than that in PIPP-Xs.

The calculated energy levels of the K* tautomers relative to the E* energy level for PIPP-Xs and PIPN are displayed in Figure 3d. The relative energy of each *cis*-K* state in PIPP-Xs is substantially lower than that in the E* state, whereas those for other K* tautomers, *per*-K* and *trans*-K*, are higher. In PIPN, meanwhile, the energy differences among E*, *cis*-K*, and *per*-K* are less than 0.5 kcal mol^{-1} (Figure 3d). Considering the calculated relative energy of each K* state in the PIPP-Xs and PIPN, we suggest that, in PIPP-Xs, the emissive K* state might be *cis*-K*, whereas in PIPN, the emissive K* state can be either *cis*-K* or *per*-K*. Particularly, in PIPN, the small energy differences among E*, *cis*-K*, and *per*-K* result in small Stokes shift. Nevertheless, the calculated vertical electronic transition energy at the *cis*-K* structure of PIPN, ΔE_v in Table S1, an estimate for the emission energy, is smaller than those of PIPP-H and PIPP-F. The discrepancy between the blue-shifted emission maxima in PIPN and the smaller calculated ΔE_v is probably caused by the bent geometry of the PD group in the optimized *cis*-K* structure, which may raise the ground-state energy level more than expected.

To elucidate the fast ESIPT dynamics of the four compounds, we measured the femtosecond TA spectra in DCM with 350 nm excitation. The results are shown in Figures 4−6 and S6. In PIPP-H, the early-time TA spectra are characterized by an intense positive signal around 440 nm and a broad positive signal over 560 nm (Figure 4a). In the late delay times (>4 ps), the negative absorption band around 510 nm are observed (Figure 4a,c). The positive and negative signals correspond to excited-state absorption (ESA) and to stimulated emission of K*, respectively. The time profiles recorded at positive signals around 440 nm and over 560 nm exhibit fast rise and decay and finally show a constant optical density (Figure 4b,d). All time profiles monitored at several wavelengths can be expressed by a tetra-exponential function with shared relaxation times of ∼0.2, 65.6, 1079 ps, and >5 ns (Table 1). Like PIPP-H, PIPP-F exhibits similar transient absorption spectra, with positive signals at approximately 440 nm and over 560 nm and a negative absorption band at around 515 nm (Figure S6). All time profiles monitored at several wavelengths can also be fit by a tetra-exponential function with

DOI: 10.1021/acs.jpcc.9b07373
J. Phys. Chem. C 2019, 123, 29116−29125

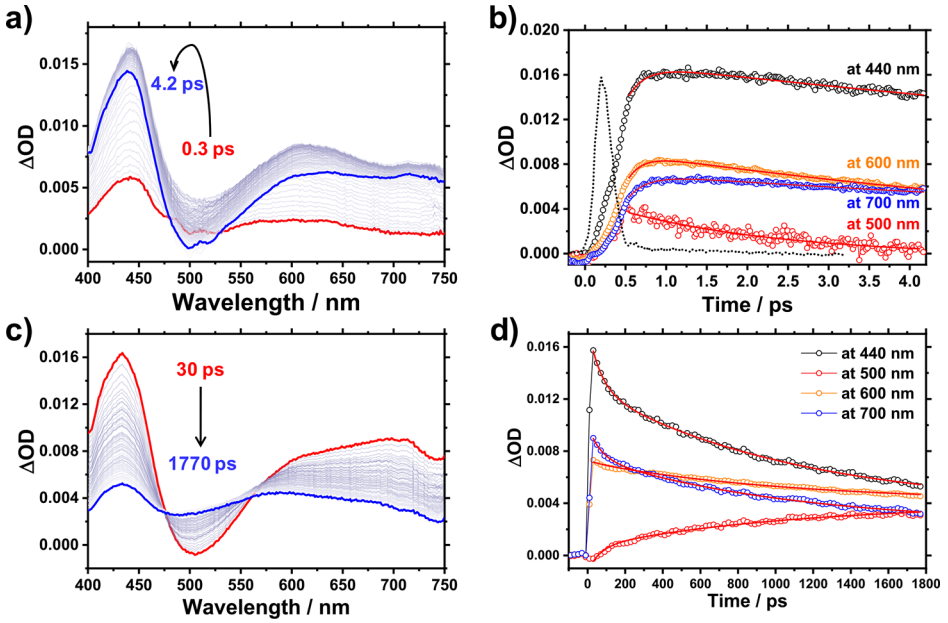

Figure 4. (a,c) Transient absorption spectra of PIPP-H in DCM. Excitation wavelength is 350 nm. (b,d) Time profiles monitored at selected wavelengths (black circle: 440 nm, red circle: 500 nm, orange circle: 600 nm, and blue circle: 700 nm). The instrument response function (IRF) is shown as a black dotted line. Theoretical fitting curves are shown as a red solid line.

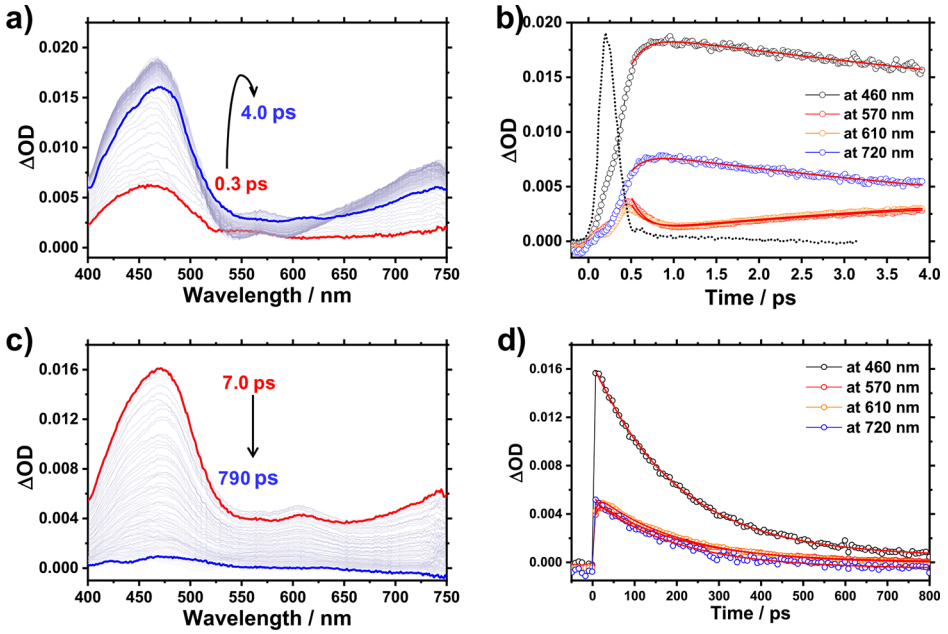

Figure 5. (a,c) Transient absorption spectra of PIPP-OMe in DCM. Excitation wavelength is 350 nm. (b,d) Time profiles monitored at selected wavelengths (black circle: 460 nm, red circle: 570 nm, orange circle: 610 nm, and blue circle: 720 nm). The IRF is shown as a black dotted line. Theoretical fitting curves are shown as a red solid line.

shared relaxation times of ~0.2, 191.6, 1142 ps, and >5 ns (Table 1). Similarly, PIPP-OMe shows an intense positive signal at around 440 nm and a broad positive signal over 500 nm (Figure 5a), without any negative signal. The absence of a negative signal may result from the strong overlap of the ESA band of PIPP-OMe and its K* emission band. Time constants for relaxations are ~0.2, 183.9, 1007 ps, and >5 ns (Table 1). By contrast, the early-time TA spectra of PIPN in DCM exhibit a broad positive signal in the range of 400−750 nm (Figure 6a). In the late delay times (>9 ps), the TA spectra are characterized by a relatively intense positive signal around 470 nm and a broad positive signal over 520 nm (Figure 6c). Interestingly, PIPN reveals a different kinetic behavior in ESIPT and subsequent relaxation processes (Figure 6b,d). As shown in Figure 6b, all time profiles monitored at several wavelengths show a rising component of ~0.2 ps. Furthermore, a fast decay component of 0.5 ps is observed at longer wavelengths (>550 nm) (Figure 6b). This fast decay component of 0.5 ps is observed only for PIPN, indicating that the excited-state dynamics of PIPN greatly differs from those of PIPP-Xs. All time profiles measured in the late delay times decayed with time constants of 47.5 and 358.3 ps and a

DOI: 10.1021/acs.jpcc.9b07373
J. Phys. Chem. C 2019, 123, 29116−29125

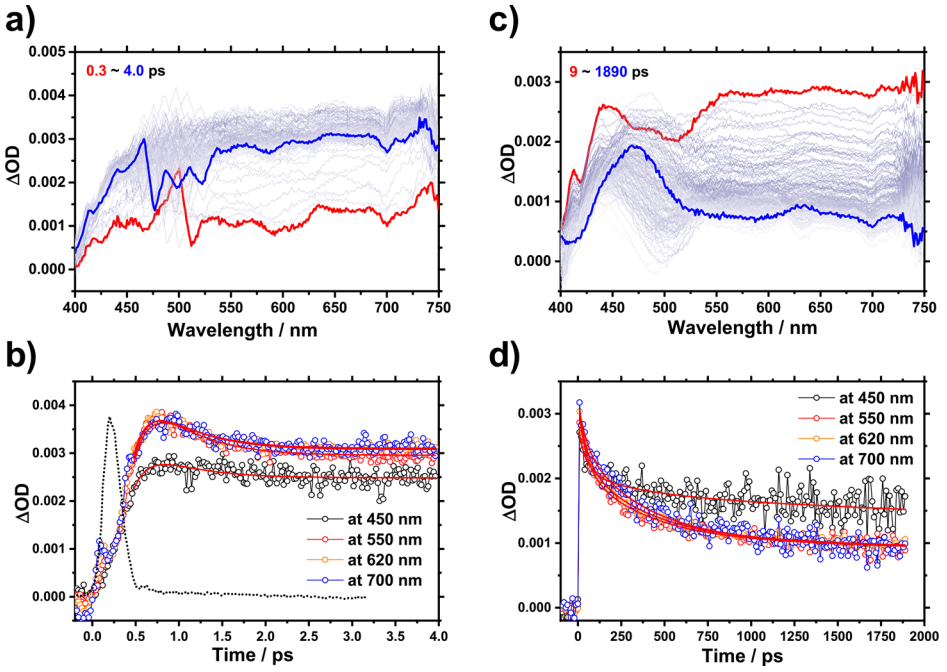

Figure 6. (a,c) Transient absorption spectra of PIPN in DCM with the excitation wavelength of 350 nm. (b,d) Decay profiles monitored at selected wavelengths (black circle: 450 nm, red circle: 550 nm, orange circle: 620 nm, and blue circle: 700 nm). The IRF is shown as a black dotted line. Theoretical fitting curves are shown as a red solid line.

Table 1. Time Constants Determined from TA Measurement (λ_{Pump} = 350 nm) for PIPP-H, PIPP-F, PIPP-OMe, and PIPN in DCM

	τ_1/ps	τ_1'/ps	τ_2/ps	τ_3/ps	τ_4
PIPP-H	<0.2		65.6 ± 4.0	1079 ± 37	constant (>5 ns)
PIPP-F	<0.2		191.6 ± 88.0	1142 ± 58	constant (>5 ns)
PIPP-OMe	<0.2		183.9 ± 8.6	1007 ± 535	constant (>5 ns)
PIPN	<0.2	0.50 ± 0.06	47.5 ± 9.9	358.3 ± 37.0	constant (>5 ns)

residual long-lived component (Figure 6d). The determined time constants for PIPP-Xs and PIPN are summarized in Table 1.

All ESIPT compounds studied in this work commonly show an ultrafast rise component of about 0.2 ps. Considering the ESIPT reaction occurring on a subpicosecond time scale and the rise feature, the dynamics of 0.2 ps (τ_1) can be assigned to the proton transfer process to form the keto tautomers. However, the ESIPT time constant of 0.2 ps is slower than that of HBT reported by Schriever et al. (60 fs).[35] The slow ESIPT rate (0.2 ps) determined in this study is probably due to the low temporal resolution (~150 fs) of our TA system, which disturbs the accurate ESIPT rate measurement. Considering the low temporal resolution (~150 fs) of our TA system, we suggest that the ESIPT reactions for four ESIPT occur faster than 0.2 ps. On one hand, the fast ESIPT reaction occurring through vibronic coupling and tunneling should result in the formation of a highly vibrationally excited *cis*-K* tautomer. Subsequently, the highly vibrationally excited keto tautomer is stabilized through the vibrational relaxation process, which comprises intramolecular vibrational relaxation and intermolecular vibrational relaxation (vibrational cooling). It is known that the vibrational relaxation occurs on a time scale of 10^{-12} s,[36] which is slightly faster than the time constants (τ_2) observed in this study. This implies that besides the vibrational relaxation, other processes may contribute to the dynamics of τ_2. Several studies on the solvation dynamics have suggested that the vibrational relaxation process including conformational relaxation and solvent reorganization occurs on the picosecond time range (10^{-12} to 10^{-10} s).[37−42] Generally, the conformational change and solvent reorganization occurs on similar time scales because the intramolecular conformational change in the excited state perturbs the orientations of the surrounding solvent molecules and then induces the solvent reorganization. For example, using femtosecond transient resonance Raman and femtosecond transient absorption spectroscopies, Tan et al. found that the vibration cooling time constants correlate well with the thermal diffusivity of the solvent and reported that the vibrational cooling and the conformational change for *trans*-4,4′-diphenylstilbene (DPS) in DCM is essentially completed within tens of picoseconds after photoexcitation.[42] This result indicates that the solvent rearrangement for DPS in DCM occurs within several tens of picoseconds. As mentioned above, the ESIPT reaction induces intramolecular charge redistribution as well as structural relaxation, resulting in large solvent rearrangement. The solvation dynamics induced by the ESIPT-related structural relaxation and charge redistribution is expected to be relatively larger and slower than that in the FC region generated by E → E* transition without structural changes. On the other hand, some studies suggested that the solvation dynamics can be modulated by orientational solute diffusion.[43−45] These previous results lead to the hypothesis that the slow solvent rearrangement induced by the rotational motion of an ESIPT molecule can contribute to the dynamics

DOI: 10.1021/acs.jpcc.9b07373
J. Phys. Chem. C 2019, 123, 29116−29125

of τ_2 observed in this study. From these points of view, we suggest that the dynamics of τ_2 originates from the vibrational relaxation and slow solvent rearrangement as well as the slow rotational motion of an ESIPT compound.

Meanwhile, τ_3 and τ_4 can be explained in terms of population relaxation from the excited state of the keto tautomer to the ground state and its excited triplet. Indeed, the τ_3 values of all four compounds are similar to the fluorescence lifetime (Figure S7). The long component (>5 ns, τ_4) observed in all ESIPT compounds may be attributed to the long-lived excited triplet state, implying that a part of the excited state of the keto tautomer is deactivated to produce the excited triplet state. To observe the long-lived triplet excited states, we measured nanosecond TA spectra of PIPP-H and PIPN in DCM. As shown in Figure S8, the transient spectra corresponding to the triplet−triplet (T−T) absorption of PIPP-H and PIPN were measured. The triplet lifetimes of PIPP-H and PIPN in DCM were determined to be 6.3 ± 0.2 and 7.7 ± 0.3 μs, respectively. This result supports our suggestion that the long-lived components (>5 ns, τ_4) observed in all ESIPT compounds are attributed to the excited triplet state formed by the ISC process.

As noted above, in PIPN, the ESIPT process and subsequent relaxation dynamics are different from those of PIPP-Xs. In particular, PIPN shows an additional fast decay component of 0.5 ps (τ_1'), which is not observed in the other compounds. As shown in Figure 3c, in PIPP-Xs (X = H, F, and OMe), the E* → *per*-K* and *cis*-K* → *per*-K* transitions are less plausible because the energy level of *per*-K* is higher than those of E* and *cis*-K*. By contrast, in PIPN, the energy level of *per*-K* is highly similar to those of E* and *cis*-K*. Therefore, the E* → *per*-K* transition may occur competitively with the E* → *cis*-K* transition. In this regard, we suggest that the kinetics of <0.2 and 0.5 ps are attributed to the E* → *cis*-K* and the E* → *per*-K* transitions, respectively. To confirm the formation of *cis*-K* and *per*-K* for PIPN, we measured time-resolved fluorescence spectra (TRFS) for PIPN in nonpolar and polar solvents, namely, *n*-hexane and DCM (Figure 7). In early times, TRFS of PIPN clearly show dual emission bands in both nonpolar *n*-hexane and polar DCM solvents; this is also observed in the steady-state fluorescence spectra (see Figure S9). Thus, short- and long-wavelength fluorescence can be assigned to emissions from E* and K*, respectively. In addition, as shown in Figure 7, the emission from K* becomes more red-shifted as the solvent polarity increases, suggesting the emissive K* state has a charge transfer characteristic. The emission lifetime of K* is significantly longer than that of E* (Figure 7). After the fast decay of the emission from E*, the maximum of the emission band from K* in DCM is further red-shifted (482 → 512 nm) during the observed time period, whereas in *n*-hexane the emission maxima of K* rarely change. Furthermore, the fluorescence decay profiles monitored at long wavelengths (>500 nm) in nonpolar *n*-hexane and polar DCM solvents are fit by a biexponential function with two time constants (0.47 ± 0.02 and 2.35 ± 0.11 ns in *n*-hexane; 0.42 ± 0.02 and 2.46 ± 0.10 ns in DCM), indicating that the long-wavelength emission band from the K* tautomer originates from two emissive states. Based on the obtained results, we suggest that the fast and slow decay times (0.42 and 2.46 ns) observed in the long-wavelength correspond to the lifetimes of *cis*-K* and *per*-K* tautomers, respectively, and that the emission from *per*-K* is affected by the solvent polarity. Here, it is worth to note that the fraction of the 0.5 ps component can be determined to be about 15% from the change in the amplitude of time profile recorded at the long wavelength (Figure 6a). This small faction is close to that calculated from two time constants for the formation of *cis*-K* and *per*-K* (<0.2 and 0.5 ps). This consistency supports that two species, *cis*-K* and *per*-K* tautomers, are formed by the parallel pathway from the E* tautomer.

On the other hand, we speculate that in contrast to PIPP-Xs, the ESIPT reaction accompanied by the large rotation of the PD group in PIPN should be greatly affected by the solution viscosity. To confirm the viscosity effect on the ESIPT and subsequent reactions, we measured the steady-state emission spectra of PIPP-H and PIPN in triacetin, which has the viscosity of 23 cP at 20 °C and compared it with that measured in DCM whose viscosity is 0.43 cP at 20 °C. As shown in Figure S10, the emission intensity of the K* tautomer of PIPN significantly decreases with the increase of the solution viscosity, whereas the emission intensity of the K* tautomer of PIPP-H is not affected by the solution viscosity. These results indicate that the ESIPT reaction for PIPN is greatly affected by the solution viscosity compared with those of PIPP-Xs. In the highly viscous solvent, the rotation of PD group for an efficient ESIPT is suppressed by the increase of the solution viscosity, and consequently, the efficiency of the ESIPT reaction is reduced. In this regard, we suggest that the decrease of the emission intensity of the K* tautomer of PIPN in triacetin is probably due to the suppression of the ESIPT reaction in the highly viscous solvent.

The large change of the θ(CCCN) values involved in the conversion from E* to *per*-K* of PIPN in the excited state is likely to result in the interruption of π-conjugation. In this regard, Douhal et al. suggested that, in the excited state, 2-(2′-hydroxyphenyl)-imidazo[1,2-*a*]pyridine (1,2-HPIP) exists as a zwitterionic ESIPT species.[46] Therefore, we cannot rule out the possibility that the *per*-K* tautomer has a zwitterionic structure, instead of a keto form structure. As shown in Figure 7, however, the emission from the *per*-K* tautomer shows a weak dependency on the solvent polarity, unlike the case of the zwitterionic structure, which shows a strong dependency on the solvent polarity and results in large Stokes shift (~11 000

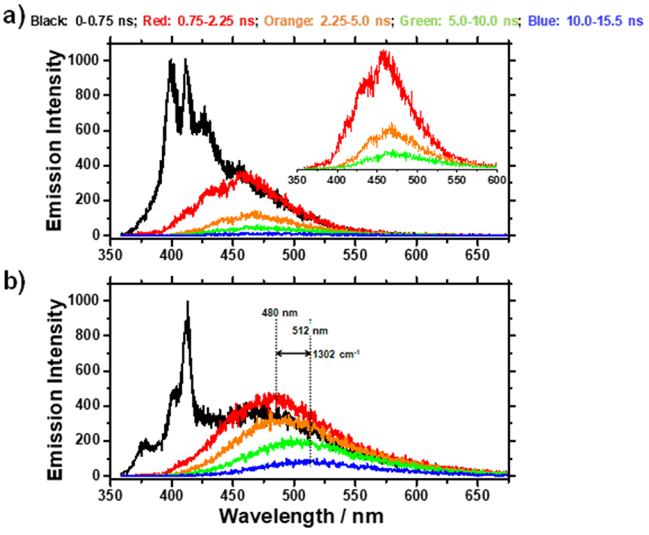

Figure 7. (a) TRFS of PIPN in *n*-hexane. Inset is enlarged view of TRFS measured at late times. (b) TRFS of PIPN in DCM.

DOI: 10.1021/acs.jpcc.9b07373
J. Phys. Chem. C 2019, 123, 29116−29125

cm^{-1}). Thus, we suggest that the *per*-K* tautomer has a twisted keto conformation rather than the zwitterionic structure suggested in other theoretical studies.[47] In TDDFT calculations for PIPN, the electronic transitions to form E*, *cis*-K*, and *per*-K* are mainly contributed by the HOMO−LUMO transition. The HOMO and LUMO at the optimized geometry of the E* and *cis*-K* tautomers are delocalized π-orbitals over the whole PA and PD groups, whereas those at the optimized geometry of *per*-K* are localized π-orbitals on each PD and PA group (Figure S11). This result indicates that the electronic transition to form *per*-K* can be attributed to the charge-transfer transition and consequently the emission from the *per*-K* state has a charge-transfer character, whereas transitions for E* and *cis*-K* are $\pi-\pi^*$ transitions. Indeed, the calculation results demonstrate that the partial charge of the naphtholate group in *per*-K* is reduced from −0.478 to −0.045 on the E* → *per*-K* tautomerization (Figure S12 and Table S2), suggesting that the formation of *per*-K* tautomer by the conformational change induces the rearrangement of the charge distribution from PA group to PD group. Sasaki et al. reported that the molecule with a pretwisted structure in the ground state can reduce the need for further twisting in the excited state.[48] Based on the obtained results, we suggest that as observed in other TICT molecules,[48,49] the formation of a *per*-K* tautomer with a CT characteristic is enhanced by its pretwisted ground state structure and the small energy difference with E*, allowing further ultrafast twisting motion in the excited state.

Additionally, on the E* → *cis*-K* tautomerization of PIPP-Xs, the substituents in PIPP-Xs, -F, and -OMe are unlikely to play as a strong modulator or charge reservoir for ICT, unlike diethyl amine and dicyanyl functional groups of the previous works. The calculated natural population analysis charges summarized in Table S2 show that the partial charges of substituents are slightly changed in the transition from E* to *cis*-K* in PIPP-Xs in contrast to a significant reduction in the PD group. For example, the partial charge of the fluorine atom of E* in PIPP-F, +0.358, is slightly lowered to +0.353 in *cis*-K*, while the partial charges of the PD group in E*, +0.023, are significantly reduced to −0.499 in *cis*-K*. Actually, the large difference of the partial charge in PD group induced by ESIPT is mainly contributed by the migration of a proton, $\delta q(H)$ = +0.539 in E* and $\delta q(H)$ = +0.496 in *cis*-K*, as shown in Table S2.

On the basis of our results, the proposed ESIPT-coupled relaxation dynamics in PIPP-Xs and PIPN are represented in Figure 8. Because of the strong intramolecular hydrogen bonding, we assume that the ground-state structures are dominant in the closed enol-form. Thus, photoexcitation preferentially induces the formation of the E* state. In PIPP-Xs, the fast ESIPT reaction (0.2 ps) due to the pre-existing intramolecular hydrogen-bonding results in efficient formation of a highly vibrationally excited *cis*-K* tautomer. The *cis*-K* state relaxes back to the ground state with large-shifted emission to the longer wavelength or to the triplet state via nonradiative intersystem crossing (ISC). Interestingly, despite the ultrafast ESIPT reaction, PIPN-OMe showed the relatively strong emission from E* compared to those of PIPP-H and PIPP-F, leading to the small I_{K^*}/I_{E^*} values. Among four compounds, the emission band from the K* tautomer for PIPP-OMe was observed at the longest wavelength (Figure 2), indicating the smallest energy gap between the ground and excited states for K*. Generally, it is known that the small

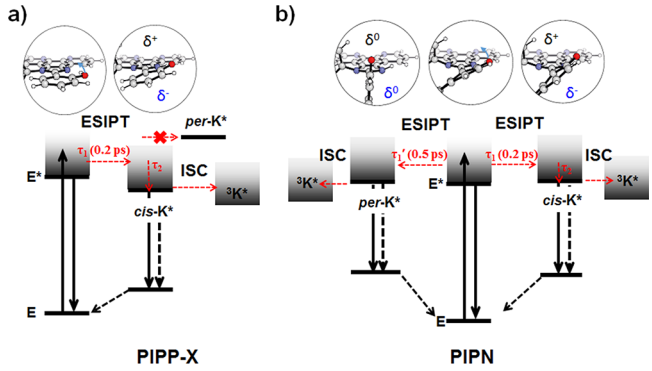

Figure 8. Schematic of ESIPT reactions in four compounds: (a) PIPP-H, PIPP-F, PIPP-OMe, and (b) PIPN. In the molecular geometries inside circles, red, blue, gray, and white colors represent the oxygen, nitrogen, carbon, and hydrogen atoms, respectively. δ^+, δ^-, and δ^0 denote the partially positive, negative, and neutral charges of PD or PA moiety.

energy gap between the ground and excited states induces predominantly the nonradiative relaxation, leading to the decrease of the emission intensity. Thus, we suggest that the small I_{K^*}/I_{E^*} ratio for PIPP-OMe is due to the low emission quantum yield (Φ_f = 0.004) and the weak emission intensity from K* tautomer owing to the small energy gap between the ground and excited states for K*. In contrast to PIPP-Xs, two K* tautomers in PIPN *cis*-K* and *per*-K* tautomers, are formed by the parallel pathway from E* tautomer generated by the photoexcitation. It is known that an excited molecule with a twisted geometry such as the *per*-K* state can be deactivated through an additional nonradiative channel, resulting in weak emission quantum yield.[47,50−53] Indeed, as shown in Table S1, the calculated energy difference (0.36 eV) between the singlet and triplet *per*-K* in PIPN is much smaller than that for PIPP-H (0.75 eV). The small energy difference may induce the fast deactivation of *per*-K* via ISC. From these points of view, we suggest that in cases of PIPN, the small I_{K^*}/I_{E^*} values may be attributed to the relatively weak emission from K* due to its twisted geometry and fast ISC, leading to the nonradiative deactivation. Finally, we conclude that the unique excited relaxation dynamics of PIPN is due to its pretwisted structure, induced by strong steric hindrance between naphthalen-2-ol and adjacent phenyl groups.

■ CONCLUSIONS

In this study, using various time-resolved spectroscopic techniques and theoretical calculations, we investigated the effects of substituent and molecular geometry on ESIPT and ICT processes for PIPP-Xs (PIPP-H, PIPP-F, and PIPP-OMe) and PIPN. Four ESIPT compounds show dual emission bands. The longer- and shorter-wavelength emissions of the four ESIPT compounds are assigned to emissions from the K* and E* conformers, respectively. The substitution of an electron-withdrawing group at the para-position of the PD group induces an efficient ESIPT reaction. Indeed, the emission intensity ratios of the E* and K* tautomers, I_{K^*}/I_{E^*}, are as follows: PIPP-F ≫ PIPP-H ≫ PIPP-OMe ≥ PIPN. This result indicates that the electron-withdrawing group rather than the electron-donating group induces efficient ESIPT. In addition, based on our calculations for the structures of PIPP-Xs and PIPN, and on our experimental results, we found that the ESIPT reaction becomes more favorable in a structure with

DOI: 10.1021/acs.jpcc.9b07373
J. Phys. Chem. C 2019, 123, 29116−29125

high planarity between the PD and PA groups than in a pretwisted structure with lower planarity. On the other hand, upon photoexcitation for PIPP-Xs, the *cis*-K* state is rapidly formed through ESIPT and then relaxes to the ground state or to the triplet state via intersystem crossing. Unlike PIPP-Xs, PIPN shows the parallel ESIPT reaction pathway accompanied by the large rotation of PD group, resulting in the formation of *cis*-K* and *per*-K* tautomers. Furthermore, the formation of *per*-K* accompanies ICT. The ICT dynamics for PIPN is due to the pretwisted structure of PIPN, which facilitates ICT. The results presented in this study demonstrate that the ESIPT and ICT dynamics is significantly affected by the molecular geometry in the ground state.

■ ASSOCIATED CONTENT

Supporting Information

The Supporting Information is available free of charge at https://pubs.acs.org/doi/10.1021/acs.jpcc.9b07373.

Experimental section; TDDFT and DFT calculated geometric and electronic excitation parameters for the ground and excited states of PIPP-H, PIPP-F, PIPP-OMe, and PIPN in DCM; ^{1}H- and ^{13}C{^{1}H}-NMR data for PIPP-H, PIPP-F, PIPP-OMe, and PIPN; transient absorption spectra and decay profiles of PIPP-F in DCM; fluorescence decay profiles for four ESIPT compounds in DCM; nanosecond transient absorption spectra and decay profiles of PIPP-H and PIPN in DCM; emission spectra of PIPN measured in various solvents; emission spectra of (a) PIPP-H and (b) PIPN in DCM and triacetin (PDF)

■ AUTHOR INFORMATION

Corresponding Authors

*E-mail: krwee@daegu.ac.kr (K.-R.W.).
*E-mail: hyotcherl.ihee@kaist.ac.kr (H.I.).

ORCID

Jungkweon Choi: 0000-0002-9979-305X
Dae Won Cho: 0000-0002-4785-069X
Kyung-Ryang Wee: 0000-0002-9923-8902
Hyotcherl Ihee: 0000-0003-0397-5965

Author Contributions

⊥J.C. and D.-S.A. contributed equally.

Notes

The authors declare no competing financial interest.

■ ACKNOWLEDGMENTS

This work was supported by IBS-R004 and Basic Science Research Program through the National Research Foundation of Korea (NRF), funded by the Ministry of Education (NRF-2017R1C1B1010736).

■ REFERENCES

(1) Wu, J.; Liu, W.; Ge, J.; Zhang, H.; Wang, P. New Sensing Mechanisms for Design of Fluorescent Chemosensors Emerging in Recent Years. *Chem. Soc. Rev.* **2011**, *40*, 3483−3495.

(2) Zhao, J.; Ji, S.; Chen, Y.; Guo, H.; Yang, P. Excited State Intramolecular Proton Transfer (ESIPT): From Principal Photophysics to the Development of New Chromophores and Applications in Fluorescent Molecular Probes and Luminescent Materials. *Phys. Chem. Chem. Phys.* **2012**, *14*, 8803−8817.

(3) Liu, B.; Wang, H.; Wang, T.; Bao, Y.; Du, F.; Tian, J.; Li, Q.; Bai, R. A New Ratiometric ESIPT Sensor for Detection of Palladium Species in Aqueous Solution. *Chem. Commun.* **2012**, *48*, 2867−2869.

(4) Henary, M. M.; Fahrni, C. J. Excited State Intramolecular Proton Transfer and Metal Ion Complexation of 2-(2′-Hydroxyphenyl)-benzazoles in Aqueous Solution. *J. Phys. Chem. A* **2002**, *106*, 5210−5220.

(5) Kwon, J. E.; Park, S. Y. Advanced Organic Optoelectronic Materials: Harnessing Excited-State Intramolecular Proton Transfer (ESIPT) Process. *Adv. Mater.* **2011**, *23*, 3615−3642.

(6) Furukawa, S.; Shono, H.; Mutai, T.; Araki, K. Colorless, Transparent, Dye-Doped Polymer Films Exhibiting Tunable Luminescence Color: Controlling the Dual-Color Luminescence of 2-(2′-Hydroxyphenyl)imidazo[1,2-a]pyridine Derivatives with the Surrounding Matrix. *ACS Appl. Mater. Interfaces* **2014**, *6*, 16065−16070.

(7) Sun, W.; Li, S.; Hu, R.; Qian, Y.; Wang, S.; Yang, G. Understanding Solvent Effects on Luminescent Properties of a Triple Fluorescent ESIPT Compound and Application for White Light Emission. *J. Phys. Chem. A* **2009**, *113*, 5888−5895.

(8) Park, S.; Kwon, J. E.; Park, S. Y. Strategic emission color tuning of highly fluorescent imidazole-based excited-state intramolecular proton transfer molecules. *Phys. Chem. Chem. Phys.* **2012**, *14*, 8878−8884.

(9) Luxami, V.; Kumar, S. Molecular half-subtractor based on 3,3′-bis(1H-benzimidazolyl-2-yl)[1,1′]binaphthalenyl-2,2′-diol. *New J. Chem.* **2008**, *32*, 2074.

(10) Chen, W.-H.; Xing, Y.; Pang, Y. A Highly Selective Pyrophosphate Sensor Based on ESIPT Turn-On in Water. *Org. Lett.* **2011**, *13*, 1362−1365.

(11) Chen, L.; Ye, J.-W.; Wang, H.-P.; Pan, M.; Yin, S.-Y.; Wei, Z.-W.; Zhang, L.-Y.; Wu, K.; Fan, Y.-N.; Su, C.-Y. Ultrafast Water Sensing and Thermal Imaging by a Metal-Organic Framework with Switchable Luminescence. *Nat. Commun.* **2017**, *8*, 15985.

(12) Yin, H.; Li, H.; Xia, G.; Ruan, C.; Shi, Y.; Wang, H.; Jin, M.; Ding, D. A Novel Non-Fluorescent Excited State Intramolecular Proton Transfer Phenomenon Induced by Intramolecular Hydrogen Bonds: An Experimental and Theoretical Investigation. *Sci. Rep.* **2016**, *6*, 19774.

(13) Padalkar, V. S.; Seki, S. Excited-State Intramolecular Proton-Transfer (ESIPT)-Inspired Solid State Emitters. *Chem. Soc. Rev.* **2016**, *45*, 169−202.

(14) Demchenko, A. P.; Tang, K.-C.; Chou, P.-T. Excited-State Proton Coupled Charge Transfer Modulated by Molecular Structure and Media Polarization. *Chem. Soc. Rev.* **2013**, *42*, 1379−1408.

(15) Gomez, E.; Alarcos, N.; Monterde, C.; Sánchez, F.; Moreno, M.; Douhal, A. Experimental and Theoretical Insights into the Influence of Electronic Density on Proton-Transfer Reactions. *Phys. Chem. Chem. Phys.* **2018**, *20*, 27149−27161.

(16) Chen, C.-L.; Chen, Y.-T.; Demchenko, A. P.; Chou, P.-T. Amino Proton Donors in Excited-State Intramolecular Proton-Transfer Reactions. *Nat. Rev. Chem.* **2018**, *2*, 131−143.

(17) Hsieh, C.-C.; Jiang, C.-M.; Chou, P.-T. Recent Experimental Advances on Excited-State Intramolecular Proton Coupled Electron Transfer Reaction. *Acc. Chem. Res.* **2010**, *43*, 1364−1374.

(18) Alarcos, N.; Cohen, B.; Ziółek, M.; Douhal, A. Photochemistry and Photophysics in Silica-Based Materials: Ultrafast and Single Molecule Spectroscopy Observation. *Chem. Rev.* **2017**, *117*, 13639−13720.

(19) Alarcos, N.; Gutierrez, M.; Liras, M.; Sánchez, F.; Douhal, A. An Abnormally Slow Proton Transfer Reaction in a Simple HBO Derivative Due to Ultrafast Intramolecular-Charge Transfer Events. *Phys. Chem. Chem. Phys.* **2015**, *17*, 16257−16269.

(20) Alarcos, N.; Gutiérrez, M.; Liras, M.; Sánchez, F.; Moreno, M.; Douhal, A. Direct Observation of Breaking of the Intramolecular H-Bond, and Slowing down of the Proton Motion and Tuning Its Mechanism in an HBO Derivative. *Phys. Chem. Chem. Phys.* **2015**, *17*, 14569−14581.

(21) Seo, J.; Kim, S.; Park, S. Y. Strong Solvatochromic Fluorescence from the Intramolecular Charge-Transfer State Created by Excited-

DOI: 10.1021/acs.jpcc.9b07373
J. Phys. Chem. C 2019, 123, 29116−29125

State Intramolecular Proton Transfer. *J. Am. Chem. Soc.* **2004**, *126*, 11154−11155.
(22) Chou, P.-T.; Liu, Y.-I.; Liu, H.-W.; Yu, W.-S. Dual Excitation Behavior of Double Proton Transfer versus Charge Transfer in 4-(N-Substituted Amino)-1H-Pyrrolo[2,3-b]Pyridines Tuned by Dielectric and Hydrogen-Bonding Perturbation. *J. Am. Chem. Soc.* **2001**, *123*, 12119−12120.
(23) Rumble, C. A.; Breffke, J.; Maroncelli, M. Solvation Dynamics and Proton Transfer in Diethylaminohydroxyflavone. *J. Phys. Chem. B* **2017**, *121*, 630−637.
(24) Germino, J. C.; Barboza, C. A.; Quites, F. J.; Vazquez, P. A. M.; Atvars, T. D. Z. Dual Emissions of Salicylidene-5-Chloroaminepyridine Due to Excited State Intramolecular Proton Transfer: Dynamic Photophysical and Theoretical Studies. *J. Phys. Chem. C* **2015**, *119*, 27666−27675.
(25) Yushchenko, D. A.; Shvadchak, V. V.; Klymchenko, A. S.; Duportail, G.; Pivovarenko, V. G.; Mély, Y. Steric Control of the Excited-State Intramolecular Proton Transfer in 3-Hydroxyquinolones: Steady-State and Time-Resolved Fluorescence Study. *J. Phys. Chem. A* **2007**, *111*, 8986−8992.
(26) Behera, S. K.; Sadhuragiri, G.; Elumalai, P.; Sathiyendiran, M.; Krishnamoorthy, G. Exclusive excited state intramolecular proton transfer from a 2-(2′-hydroxyphenyl)benzimidazole derivative. *RSC Adv.* **2016**, *6*, 59708−59717.
(27) Su, J.; Lu, Y.; Ding, G.; Wang, Z.; Huang, F.; Gao, F.; Luo, Z.; Li, H. Pure Space Steric Hindrance Effect on Intramolecular Proton Transfer in Excited State and Photophysics of Conjugated New Dyes under Near-IR Laser Irradiation. *Dyes Pigm.* **2017**, *146*, 92−102.
(28) Iijima, T.; Momotake, A.; Shinohara, Y.; Sato, T.; Nishimura, Y.; Arai, T. Excited-State Intramolecular Proton Transfer of Naphthalene-Fused 2-(2′-Hydroxyaryl)benzazole Family. *J. Phys. Chem. A* **2010**, *114*, 1603−1609.
(29) Heller, A.; Williams, D. L. Intramolecular Proton Transfer Reactions in Excited Fluorescent Compounds. *J. Phys. Chem.* **1970**, *74*, 4473−4480.
(30) Nakagaki, R.; Kobayashi, T.; Nagakura, S. Luminescence Properties and the Primary Process of Photochromism of 2-(2-Hydroxyphenyl)Benzothiazole. *Bull. Chem. Soc. Jpn.* **1978**, *51*, 1671−1675.
(31) Itoh, M.; Fujiwara, Y. Transient absorption and two-step laser excitation fluorescence studies of photoisomerization in 2-(2-hydroxyphenyl)benzoxazole and 2-(2-hydroxyphenyl)benzothiazole. *J. Am. Chem. Soc.* **1985**, *107*, 1561−1565.
(32) Tero-Kubota, S.; Akiyama, K.; Shoji, F.; Ikegami, Y. Excited triplet state generated from excited state intramolecular proton transfer in 2-(2′-hydroxyphenyl)benzothiazole. *J. Chem. Soc., Chem. Commun.* **1992**, 641−643.
(33) Roberts, E. L.; Dey, J.; Warner, I. M. Excited-State Intramolecular Proton Transfer of 2-(2′-Hydroxyphenyl)-benzimidazole in Cyclodextrins and Binary Solvent Mixtures. *J. Phys. Chem. A* **1997**, *101*, 5296−5301.
(34) Ogoshi, T.; Miyake, J.; Chujo, Y. Multiresponsive Photopatterning Organic−Inorganic Polymer Hybrids Using a Caged Photoluminescence Compound. *Macromolecules* **2005**, *38*, 4425−4431.
(35) Schriever, C.; Barbatti, M.; Stock, K.; Aquino, A. J. A.; Tunega, D.; Lochbrunner, S.; Riedle, E.; de Vivie-Riedle, R.; Lischka, H. The Interplay of Skeletal Deformations and Ultrafast Excited-State Intramolecular Proton Transfer: Experimental and Theoretical Investigation of 10-Hydroxybenzo[h]Quinoline. *Chem. Phys.* **2008**, *347*, 446−461.
(36) Lakowicz, J. R. Principles of Fluorescence Spectroscopy. *Solvent and Environmental Effects*, 3rd ed.; Springer Science+Business Media, LLC, 2010; pp 205−236.
(37) Oxtoby, D. W. Dephasing of Molecular Vibrations in Liquids. *Advances in Chemical Physics*; John Wiley & Sons, Ltd, 1979; Vol. *40*, pp 1−48.
(38) Elsaesser, T.; Kaiser, W. Vibrational and Vibronic Relaxation of Large Polyatomic Molecules in Liquids. *Annu. Rev. Phys. Chem.* **1991**, *42*, 83−107.
(39) Owrutsky, J.; Raftery, D.; Hochstrasser, R. M. Vibrational Relaxation Dynamics in Liquids. *Annu. Rev. Phys. Chem.* **1994**, *45*, 519−555.
(40) Rückert, I.; Demeter, A.; Morawski, O.; Kühnle, W.; Tauer, E.; Zachariasse, K. A. Internal Conversion in 1-Aminonaphthalenes. Influence of Amino Twist Angle. *J. Phys. Chem. A* **1999**, *103*, 1958−1966.
(41) Iwata, K.; Hamaguchi, H.-o. Microscopic Mechanism of Solute−Solvent Energy Dissipation Probed by Picosecond Time-Resolved Raman Spectroscopy. *J. Phys. Chem. A* **1997**, *101*, 632−637.
(42) Tan, X.; Gustafson, T. L.; Lefumeux, C.; Burdzinski, G.; Buntinx, G.; Poizat, O. Solvation Dynamics Probed by Femtosecond Transient Absorption Spectroscopy: Vibrational Cooling and Conformational Relaxation in S1trans-4,4′-Diphenylstibene†. *J. Phys. Chem. A* **2002**, *106*, 3593−3598.
(43) Sajadi, M.; Weinberger, M.; Wagenknecht, H.-A.; Ernsting, N. P. Polar Solvation Dynamics in Water and Methanol: Search for Molecularity. *Phys. Chem. Chem. Phys.* **2011**, *13*, 17768−17774.
(44) Bagchi, B.; Oxtoby, D. W.; Fleming, G. R. Theory of the Time Development of the Stokes Shift in Polar Media. *Chem. Phys.* **1984**, *86*, 257−267.
(45) Kumar, P. V.; Maroncelli, M. Polar Solvation Dynamics of Polyatomic Solutes: Simulation Studies in Acetonitrile and Methanol. *J. Chem. Phys.* **1995**, *103*, 3038−3060.
(46) Douhal, A.; Amat-Guerri, F.; Acuna, A. U. Photoinduced Intramolecular Proton Transfer and Charge Redistribution in Imidazopyridines. *J. Phys. Chem.* **1995**, *99*, 76−80.
(47) Barbatti, M.; Aquino, A. J. A.; Lischka, H.; Schriever, C.; Lochbrunner, S.; Riedle, E. Ultrafast internal conversion pathway and mechanism in 2-(2′-hydroxyphenyl)benzothiazole: a case study for excited-state intramolecular proton transfer systems. *Phys. Chem. Chem. Phys.* **2009**, *11*, 1406−1415.
(48) Sasaki, S.; Drummen, G. P. C.; Konishi, G.-i. Recent advances in twisted intramolecular charge transfer (TICT) fluorescence and related phenomena in materials chemistry. *J. Mater. Chem. C* **2016**, *4*, 2731−2743.
(49) Choi, J.; Ahn, D.-S.; Oang, K. Y.; Cho, D. W.; Ihee, H. Charge Transfer-Induced Torsional Dynamics in the Excited State of 2,6-Bis(Diphenylamino)Anthraquinone. *J. Phys. Chem. C* **2017**, *121*, 24317−24323.
(50) Potter, C. A. S.; Brown, R. G.; Vollmer, F.; Rettig, W. Role of twisted intramolecular charge-transfer states in the decay of 2-(2′-hydroxyphenyl)benzothiazole following excited-state intramolecular proton transfer. *J. Chem. Soc., Faraday Trans.* **1994**, *90*, 59−67.
(51) Guallar, V.; Moreno, M.; Lluch, J. M.; Amat-Guerri, F.; Douhal, A. H-Atom Transfer and Rotational Processes in the Ground and First Singlet Excited Electronic States of 2-(2′-Hydroxyphenyl)oxazole Derivatives: Experimental and Theoretical Studies†. *J. Phys. Chem.* **1996**, *100*, 19789−19794.
(52) Kim, S.; Seo, J.; Park, S. Y. Torsion-Induced Fluorescence Quenching in Excited-State Intramolecular Proton Transfer (ESIPT) Dyes. *J. Photochem. Photobiol., A* **2007**, *191*, 19−24.
(53) Böhnke, H.; Bahrenburg, J.; Ma, X.; Röttger, K.; Näther, C.; Rode, M. F.; Sobolewski, A. L.; Temps, F. Ultrafast Dynamics of the ESIPT Photoswitch N-(3-Pyridinyl)-2-Pyridinecarboxamide. *Phys. Chem. Chem. Phys.* **2018**, *20*, 2646−2655.

DOI: 10.1021/acs.jpcc.9b07373
J. Phys. Chem. C 2019, 123, 29116−29125